Biophysical Journal, Volume 97

Supporting Material

Synchronous In Situ ATPase activity, Mechanics and Ca^{2+} Sensitivity of Human and Porcine Myocardium.

Peter John Griffiths, Radek Pelc, Henrik Isackson, Charles S. Redwood, Sérgio S. Funari, Hugh Watkins, and Christopher C. Ashley

Supplementary Material

S.1. Preparations.

Flash frozen human myocardium: a short (ca. 5mm) segment of tissue was dissected from the sample, whilst frozen, along the predominant axis of orientation of the cardiac cells and placed in a Ca^{2+}-free ATP (relaxing) solution containing 1% Triton X100 to disrupt membrane systems plus the muscle relaxant BDM (butane-2,3-dione monoxime; 20mM, Sigma Aldrich, Poole, Dorset, U.K.) to suppress contractile activity. The segment was pared-down until thinner segments of 200-400μm diameter and 3-5mm in length were obtained, which were incubated in the Triton solution for 24 hours at 4°C before use. *Pig hearts* were obtained from Large White pigs within 30 minutes of death at a local abattoir. For glycerination, hearts were placed in a Tyrode's solution (NaCl, 148; KCl, 5.4; $CaCl_2$, 1.8; $MgCl_2$, 1; HEPES, 15; Glucose, 5.5; NaH_2PO_4, 0.4; NaOH, 7.15, all in mM; pH 7.4) and transported to the laboratory in ice. Trabeculae from the ventricles were cut into strips 50mm long, 5mm wide and attached at their ends to short wooden sticks. The strips were then washed in ice cold relaxing solution and placed in a bathing solution (Na_2ATP, 7; Imidazole, 10; $MgCl_2$, 8; EGTA, 5; sodium propionate, 70; BDM, 10, NaN_3, 1.5; NaOH, 18.7, all mM, Triton X100, 1%, pH 7.0, ionic strength, 128mM) containing Roche EDTA-free Complete protease inhibitor cocktail ($7g.l^{-1}$) for 2 hours at room temperature, then transferred to a storage solution (composition as for bathing solution, except 109mM potassium propionate replaced sodium propionate, KOH replaced NaOH, Triton was omitted and the solvent contained 50% glycerol) for 24 hours at 4°C. The muscle strips were then stored at -25°C. For *flash frozen porcine tissue*, hearts were immediately dissected at the abattoir and strips of trabeculae (ca. 20mm long, 5mm diameter, corresponding to the dimensions of the flash frozen human tissue at our disposal) were removed from the left ventricle and immersed in 1l of liquid nitrogen. Muscle segments for experiments were then dissected and permeabilised in the same manner as for human muscle. The long exposure to Triton reduced the resting ATPase activity in both human and porcine preparations and which was insensitive to thapsigargin (20μM), cyclopiazonic acid (400μM), azide (10mM) and ouabain (500μM). A similar relaxed ATPase activity was reported by Kentish and Stienen (1) in rat heart. In addition, we found that preparations skinned for shorter intervals (<4 hours) retained a force response when exposed to relaxing solution plus 10mM caffeine, suggesting a functioning sarcoplasmic reticulum.

S.2. Myocardial ATPase activity measurement.

To excite fluorescence, muscle segments were exposed to ultraviolet (uv) radiation from a high intensity uv LED (NCCU033(T), Nichia Corporation, Tokushima 774-8601, Japan). The uv radiation (λ=365nm at 100mW, spectrum half width (FWHM) 8nm) was transmitted through a liquid light guide to a diode housing which fitted tightly over the experimental chambers. Near the aperture of the light guide, a fused silica cylindrical lens was used to collimate the UV light beam and project a uniform light field into a 4mm wide slot enclosing the experimental chamber. On either side of the slot walls (i.e. perpendicular to the incident light beam) were mounted blue-enhanced photodiodes (OSD5.8-7Q, RS Components, Northampton, U.K.) within 2mm from the surface of the muscle segment to maximise the solid angle of fluorescent radiation accepted at the diode active surface. One diode was covered by an optical band-pass filter with a peak transmittance at 440nm, half peak bandwidth (FWHM) 46nm. The other diode was covered by a long-pass filter transmitting radiation at wavelengths greater than 600nm. In addition, a UV photodiode (S1226 18BU, Hamamatsu Photonics K.K., Hamamatsu City, 435-8558 Japan) was mounted at the end of the collimating lens to monitor source intensity. For some experiments, the long-pass filter was replaced by a 550nm filter (20nm bandwidth). The horizontal half width of the diode response to a point light source in the chamber was 6mm. The base of the experimental chambers was cut below the level of its glass windows and coated with black epoxy to prevent any fluorescence or reflection from the chamber base reaching the photodiodes. The diode housing was mounted on the aluminium arm bearing the force transducer so that, during solution exchange, the position of the muscle did not alter with respect to either the photodiodes or the liquid light guide. The optical arrangement of components is shown in fig. S1.

Practically, this device is simpler, more compact, economical and flexible than the equipment as originally conceived (2) which required an epifluorescence microscope, a xenon lamp to provide the excitation beam, and photomultiplier tubes to measure fluorescence intensity. By applying advances in UV LED technology and the advent of enhanced blue sensitivity diodes, excitation and measurement of fluorescence and the design of the device are greatly simplified. In addition, the present device has the advantage that fluorescence is excited and detected from the whole length of the muscle segment, reducing sensitivity to movement or changes in preparation length.

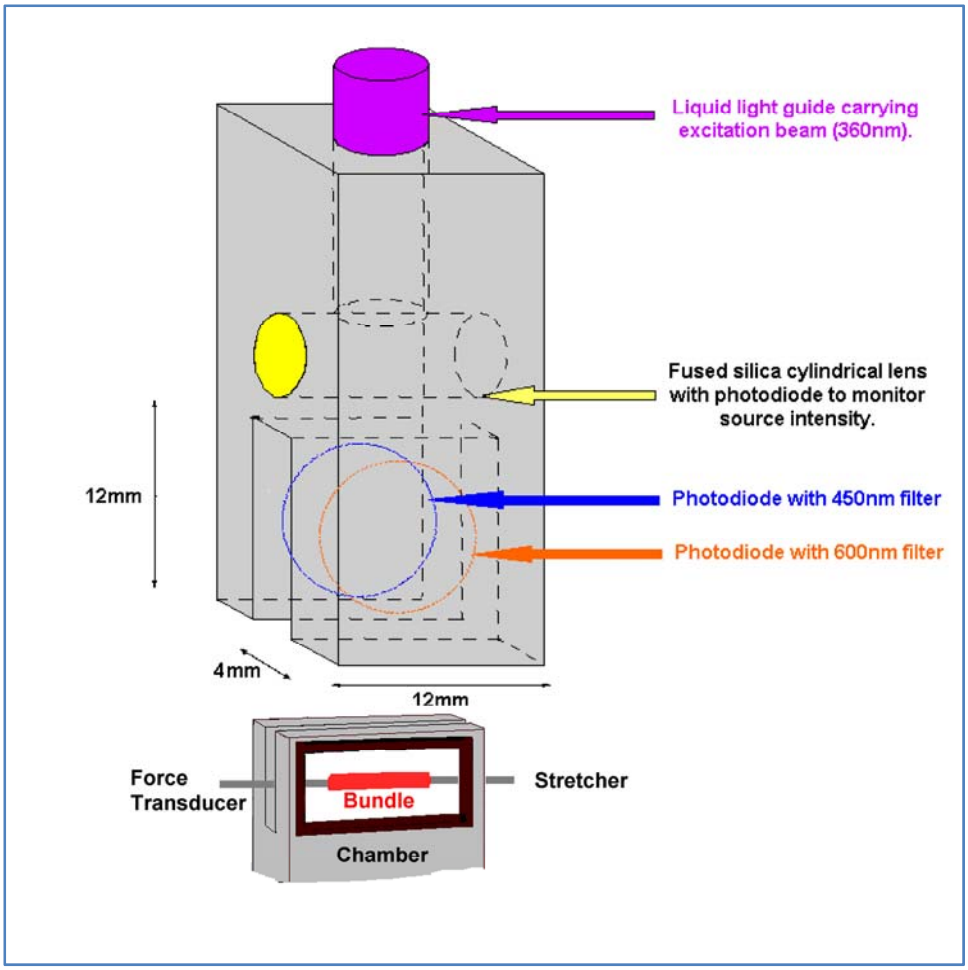

Figure S1: the experimental chambers, shown at the bottom of the picture, consist of two parallel glass plates 1.5mm apart, and fit into the 6mm slot in the base of the diode housing (shown above the chamber). The ends of the chambers are open, to allow insertion of stainless steel rods connected to the force transducer and the stretcher motor, and solutions were retained within the chamber by surface tension. The fused silica cylindrical lens serves to collimate the exciting beam near the aperture of the light guide to produce a uniform light field inside the slot. On the inside surface of the slot walls are mounted photodiodes, one detecting radiation at 450nm (NADH fluorescence), the other monitoring intensity at wavelengths greater than 600nm (used to check for non-specific fluorescence intensity changes). Source intensity is monitored by a UV photodiode mounted at the edge of the cylindrical lens.

ATPase activity measurements in human myocardium were obtained as for porcine tissue. An example is shown in fig. S2.

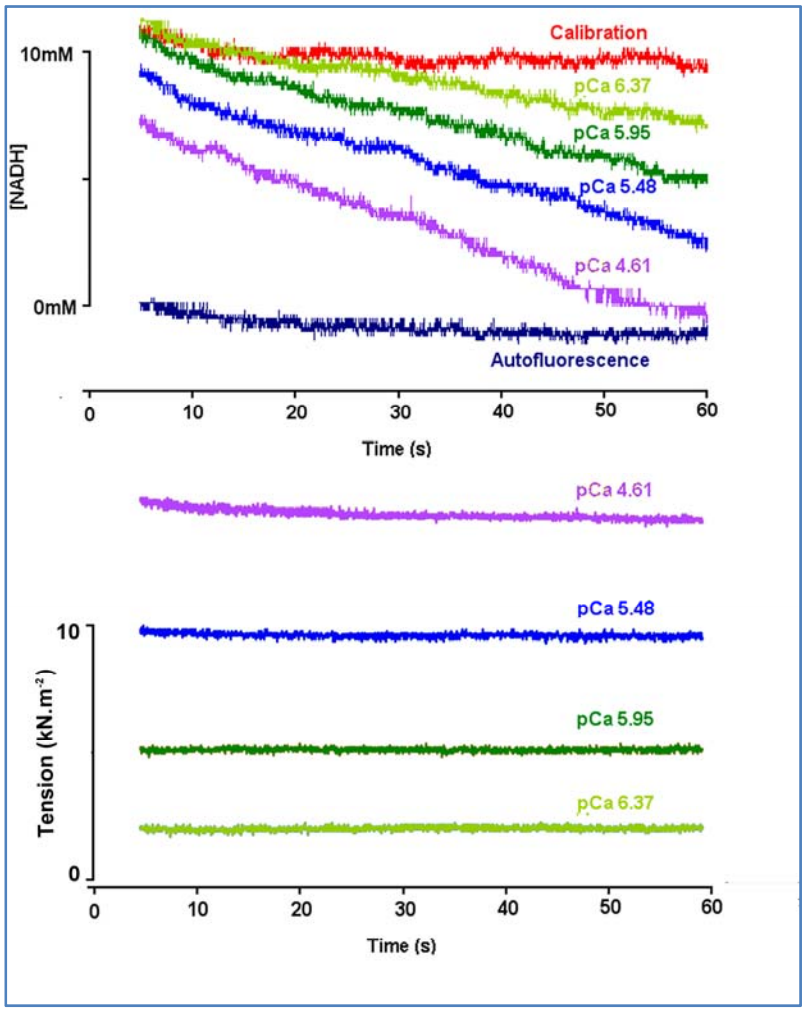

Figure S2. ATPase activity measured in human myocardium, equivalent to fig. 2 in the main text. Bundle diameter; 250µm. Temperature, 28°C. The smaller human preparation gives a noisier fluorescence signal and does not show flattening of the fluorescence decline at the lowest pCa due to NADH depletion and evident in fig. 2.

Our ATPase assay system permits simultaneous recording of force and ATPase activity from functionally intact myofibrils, thus the constraints of load and shortening on myosin turnover kinetics are automatically included in the measurements, which is not possible when myosin ATPase activity is studied in solution (3). An alternative approach is to measure NADH absorbance in the bathing solution surrounding a fibre of tissue, either by transfer to a measuring cuvette (4) or directly in the experimental chamber (5). These techniques take into account mechanical constraints on the actomyosin ATPase cycle and have the advantage that tissue NADH is replenished throughout the measurement period, but they are limited in time resolution by the diffusion delay of NADH equilibrium with the bulk medium and by the smaller sensitivity to quantities of NADH consumed. Furthermore, they require an estimate of tissue volume in order to convert the quantity of NADH consumed into ATP consumption rate inside the tissue, a potential source of significant error if tissue cross-section is irregular. Instead, NADH fluorescence measurements within the tissue volume automatically yield data as concentration changes, do not require equilibration with the bulk

medium, and are much more sensitive to NADH consumption, since the same quantity of NADH consumed produces a larger concentration change in the tissue than it could in the bulk medium. The present experiments have the additional advantage over our previous study (using 340nm excitation (2)) that, because NADH absorbance and light attenuation by the tissue are smaller at 365nm, light penetrates further to the core of the bundle and ATP consumption over the whole bundle volume is better averaged as a result. At the emission wavelength (450nm), light attenuation by the tissue was 75% of that at 365nm. Whereas tissue scattering and NADH absorption are important components of the exciting beam attenuation, if the emitted beam is scattered equally in all directions, then only light absorbance by the tissue affects emitted intensity, which comprises only a part of the tissue light attenuation at 450nm. Incident light attenuation is therefore the more important factor in the ATPase and diffusion measurements, and we have ignored emitted radiation absorbance effects.

To test the efficacy of our *in situ* ATPase assay, we compared results with cuvette assays in four porcine preparations. For cuvette ATPase assays, preparations were first transferred to 80μl of the chosen solution (of the same composition as used in the *in situ* ATPase assays), and when force had stabilised, then transferred into fresh solution of the same composition and incubated for 600-800s. Simultaneously, a second chamber was used to incubate the same volume of solution without exposure to the preparation. This chamber then acted as a control against which the consumption of NADH by the preparation could be assessed. The solutions from both the test and the control chambers were then transferred to 1ml of distilled water, plus three washings of each of the chambers, and the absorbance of the solutions at 340nm was measured on a Perkin-Elmer Lambda5 spectrophotometer (PerkinElmer Inc., 940 Winter Street, Waltham, Massachusetts 02451, U.S.A.). The difference in extinction between control and test was used to calculate the amount of NADH consumed as a result of ATPase activity in the preparation.

S.3. Diffusion Coefficient Estimation.

We define fluorescence intensity (I([C],t)) as:

$$I([C],t) = [C(x,y,t)]E([C],x,y) \qquad (S1)$$

Where [C(x,y,t)] is the concentration at time t for the point x,y in the tissue and E([C],x,y) is the excitation intensity at that point and concentration. This is obtained from the extinction coefficient NADH plus the light attenuation by the tissue, such that

$$E([C],x,y) = \exp(-\{\varepsilon \ln(10)[C(x,y,t)] + F\}x) \qquad (S2)$$

ε being the extinction coefficient of NADH at λ=365nm (taken as $3.17 mM^{-1}.cm^{-1}$). *F* is the intrinsic light attenuation by the muscle tissue, caused by absorption and scattering. We estimated *F* from a sheet of myocardium trapped between two UV-transparent plastic plates. The plates were held together by rubber O-rings placed round the plate ends, and the cavity

between the plates was filled with relaxing solution. Light extinction was then measured in a spectrophotometer. The length and width of the trapped tissue were recorded, the tissue weighed, and the thickness of tissue in the light path calculated using a tissue density of 1040kg.m^{-3}. In addition, we measured the light path directly by observing the separation between the two plastic plates microscopically. The two estimates of light path were in good agreement. The effect of light attenuation by the tissue is to reduce fluorescence from the tissue core, causing NADH fluorescence during loading to approach its final level more rapidly than concentration. The preparations used were not perfectly circular in cross-section, therefore we calculated the concentration term either for a cylinder or for a rectangular cross-section body: in the case of a cylinder of radius a at a distance r from the axis, $r = (x^2 + y^2)^{½}$, surface concentration $[C(a)]$,

$$[C(r,t)] = [C(a)]\left(1 - \frac{2}{a}\sum_{n=1}^{15} exp(-D\alpha_n^2 t)\frac{J_0(r\alpha_n)}{\alpha_n J_1(\alpha_n a)}\right) \qquad (S3)$$

where J_0 and J_1 are Bessel functions of the first kind of order 0 and 1, respectively. For a body of rectangular cross-section at a point with coordinates x, y measured from the surfaces at x=0 and y=0 to surfaces at $x=l_x$ and $y=l_y$, with concentration $[C(x_0,y_0)]$ at all surfaces:

$$[C(x,y,t)] = [C(x_0,y_0)]\left[1 - \frac{16}{\pi}\sum_{n=0}^{5}\sum_{m=0}^{5}\left\{\frac{1}{2n+1}sin\left(\frac{\{2n+1)\pi x}{l_x}\right)exp\left(\frac{-Dt(2n+1)^2\pi^2}{l_x^2}\right)\right\} \times \left\{\frac{1}{2m+1}sin\left(\frac{\{2m+1)\pi y}{l_y}\right)exp\left(\frac{-Dt(2m+1)^2\pi^2}{l_y^2}\right)\right\}\right] \qquad (S4)$$

Because E([C],r) or E([C],x,y) is itself a function of concentration, its contribution to I([C],t) has to be evaluated numerically, using:

$$dE/dx = -E([C],x,y)\{\varepsilon ln(10)[C(x,y,t)] + F\} \qquad (S5)$$

For computation of the concentration distribution and fluorescence of NADH when the rate of consumption (V) and replenishment by diffusion are at steady state, we used the equation for steady state in a cylinder of radius a:

$$\frac{d}{dr}\left(r\frac{d[C]}{dr}\right) = \frac{Vr}{D} \qquad (S6)$$

to obtain:

$$[C(r)] = [C(a)] - \frac{V(a^2 - r^2)}{4D} \qquad (S7)$$

This equation can be used to replace the concentration terms in eqns. S1 and S2 to obtain fluorescence intensity, I([C]).

In addition to measuring the NADH diffusion coefficient, in three preparations we also investigated the radial diffusion of 155kDa tetramethylrhodamine (TMR) dextran (Sigma

Aldrich, comparable in molecular weight to LDH) into the cardiac tissue by monitoring fluorescence at 550nm for loading times from 10 to 4000s. The loading medium was relaxing solution plus 2% TMR dextran and CrP/K. The loading data was fitted for *D* in the same manner as for NADH using a dextran extinction coefficient of 13,846$mM^{-1}.m^{-1}$ at 365nm. We obtained values for *D* having a mean of 1.12±0.27 x10^{-11} $m^2.s^{-1}$ for the cylindrical diffusion model, equivalent to a loading half time of 127s for a 300μm diameter fibre bundle. Figure S3 shows the time course of fluorescence increase during loading with 10mM NADH (upper panel) or 2% 155kDa tetramethylrhodamine dextran (lower panel).

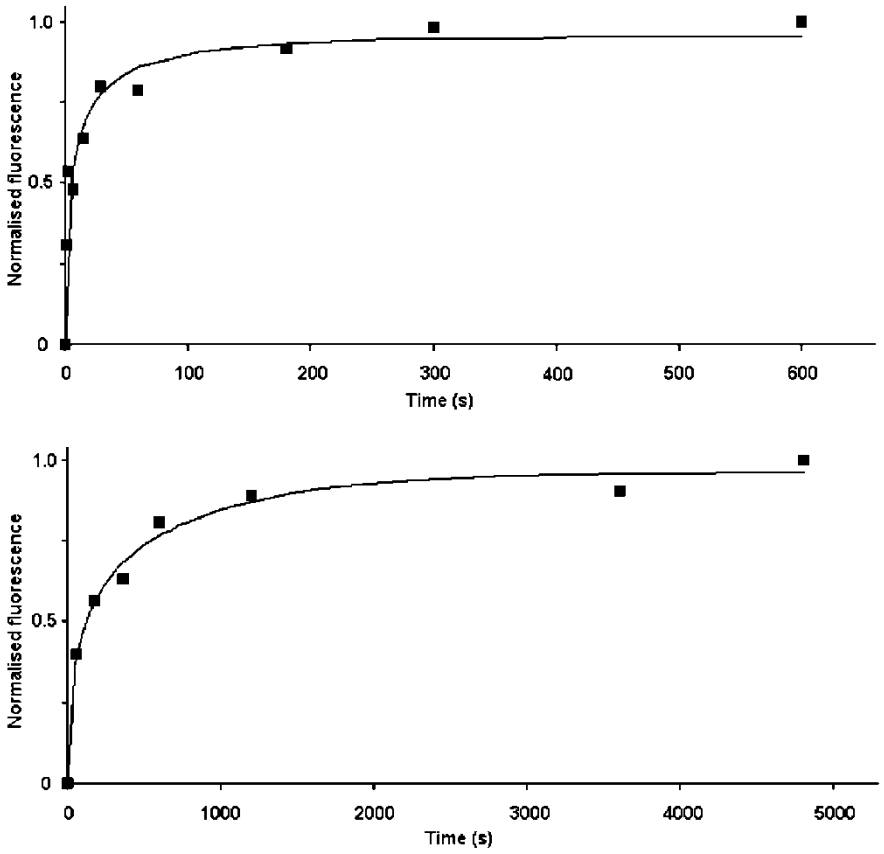

Figure S3: top panel; fluorescence intensity against loading time for 10mM NADH in relaxing solution plus CrP/K for glycerinated porcine myocardium. Continuous line; best fit for eqn. S1 to the data points for the model A(I([C(r)],t)-B), adjusting the diffusion coefficient (*D* in eqn. S3) and the scaling and autofluorescence constants A and B. Lower panel; fluorescence against loading time for 2% 155kDa tetramethylrhodamine dextran for glycerinated porcine myocardium.

Empirically, the Stokes-Einstein relation predicts that *D* is inversely proportional to the cube root of molecular weight. PEP, having a molecular weight only 28% that of NADH (663Da), would thus be expected to have a 1.5 fold higher diffusion coefficient, preventing development of a rigor core even in conditions of NADH starvation. A similar argument applies also to ATP regeneration from creatine phosphate, which has a molecular weight 44% that of NADH and an expected 1.3 fold higher diffusion coefficient. The halftime (127s) for 155kDa dextran loading should be close to that of LDH, which is of a similar size (140kDa).

According to the Stokes-Einstein relation, its *D* value should be ca. one sixth of that determined for NADH. Its measured value is three fold smaller than this, probably because the molecular dimensions of the molecule approach those of the spacings in the myofilament lattice. PK, which has a molecular weight of 237kDa, is likely to load the fibre bundle even more slowly than LDH, but we were unable to find a form of labelled dextran of similar molecular weight with which to estimate its diffusion time course. Prolonged incubation with a heavier (500kDa) fluorescent dextran showed no evidence of uptake, indicating that its molecular dimensions excluded it completely from the lattice. But the similarity of the force-pCa curves using CrP/K and PK/LDH suggests that PK does enter the tissue in sufficient amounts during pre-incubation before the experiment, otherwise ATP starvation would alter the force-pCa curve compared to that obtained using the alternative and smaller regenerating enzyme, creatine kinase. Similarly, absence of an effect on ATPase activity measurements on reducing PK/LDH to 250U.ml^{-1} shows that PK activity is not limiting in NADH consumption rates.

By applying eqn. S7 to a human preparation showing a maximum total ATPase activity of 132μM.s^{-1} and assuming cylindrical symmetry, one can calculate the steady state NADH distribution and its fluorescence contribution (eqn. S1). This is shown for bundles of 200 to 400μm diameter in the upper panel of fig. S4, taking external NADH as 10mM.

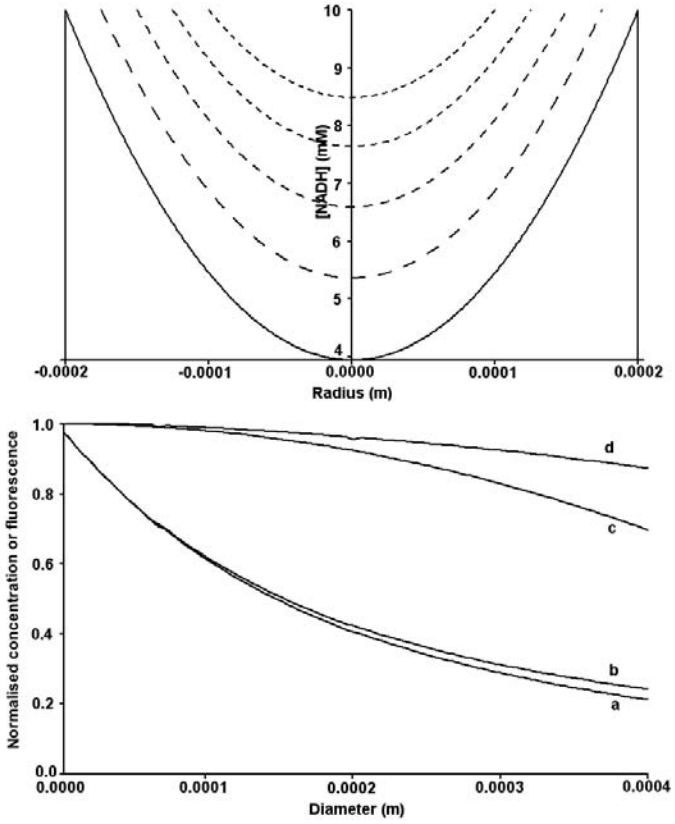

Figure S4: top panel; radial concentration distribution of NADH for an ATPase activity of 132μM.s^{-1}, using an NADH diffusion coefficient of 2.18x10^{-10}m^2.s^{-1} and 10mM as the surface [NADH]. Lower panel; effects on fluorescence signals of exciting light absorbance by NADH and attenuation by the tissue. Line a, calculated

initial NADH fluorescence signal in figs. 2 or S2, including the effects of light attenuation and NADH consumption, normalised to an ideal NADH fluorescence without light attenuation and NADH consumption. Line b, fluorescence in the absence of consumption (i.e. the calibration signal in figs. 2 and S2), normalised to the ideal signal amplitude in the absence of any light attenuation. Line d is the ratio of line a to line b, corresponding to the [NADH] that would be estimated by a fluorescence measurement immediately after transfer into liquid paraffin. Line c is the true [NADH] averaged over the whole bundle radius for this consumption rate as a fraction of external [NADH] in the absence of consumption and distributed uniformly.

Because diffusion is insufficiently rapid to replenish NADH at the bundle core, [NADH] declines towards the centre of the bundle, and this effect becomes more pronounced as diameter increases, accounting for the fall in fluorescence at low pCa at the far left of figures 2 and S2 compared to calibration solution. The lower panel of Fig. S4 shows the consequences of this radial concentration gradient plus the effect of attenuation of exciting light intensity on [NADH] estimated from fluorescence. Curve a shows the fluorescence intensity expected from a cylinder of myocardium as a function of diameter for the ATPase activity and radial [NADH] distributions in the upper panel, taking into account light attenuation by the tissue and by NADH absorbance, and also consumption of NADH by ATPase activity. The intensity has been normalised to that expected for a uniform radial distribution of NADH equal to the external concentration (10mM) in the absence of both consumption and light attenuation. Line b is the corresponding normalised intensity for the calibration solution, i.e. in the absence of NADH consumption but including light attenuation. The ratio of these two curves corresponds to estimation of the average [NADH] in the tissue from the ratio of the heights above autofluorescence of the signals at different pCa's to the calibration signal (the method of calculation of the rate of NADH consumption in eqn. 3), and is shown in curve d. Curve c is the true average [NADH], computed by integrating the [NADH] distributions in the upper panel of fig. S4 over the whole bundle cross-section for each bundle diameter. Comparison of curves c and d shows that the combined effects of light attenuation and NADH consumption cause [NADH] calculated from fluorescence to be overestimated by up to 15%, depending on the bundle diameter. ATPase activity measurements are calculated from the rate at which curve d intensity declines after transfer into liquid paraffin. Because diffusion is fast compared to consumption, radial concentration gradients will tend to dissipate quickly after transfer and average [NADH] in the bundle will fall due to NADH consumption. The resultant reduction in light absorbed by NADH increases the exciting light intensity able to penetrate to the core of the bundle. The effects of these events on the ATPase assay are illustrated in fig.S5

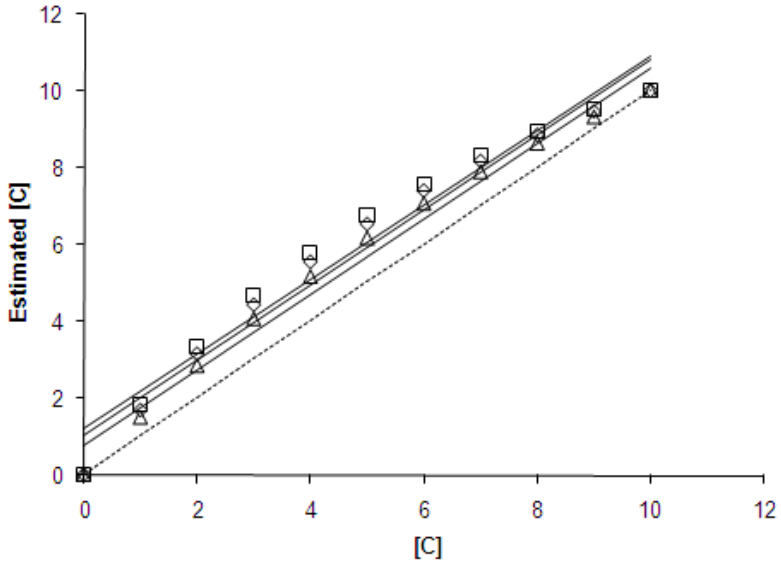

Figure S5: dependence of fluorescence signal intensity on [NADH], calculated for zero attenuation of the exciting beam (dotted line) and for attenuation by fibre and NADH absorbance in bundles of 200 (triangles), 300 (diamonds) and 400µm (squares) diameter for a uniform radial concentration distribution of NADH. Continuous lines show linear regressions of the data points for the different bundle diameters.

The estimated [NADH] from fluorescence is plotted against true [NADH] for uniform radial concentration distributions in bundles of 200, 300 and 400µm diameter. In the ideal case (no light attenuation), the slope of the relation should be unity (dotted line), whereas a linear regression of actual fluorescence upon [NADH] gives slopes of 0.984, 0.978 and 0.969, respectively. For a linear fall in true [NADH] with time, linear regression of NADH fluorescence upon time would therefore underestimate true ATPase activity by 1.5-3.1%

S.4. Ultrastructural Studies.

We assessed the structural condition and the fractional volume occupancy of frozen tissue using strips of tissue taken directly from the unskinned samples. Cryopreserved human and porcine myocardium were fixed in 0.1M phosphate buffer (pH 7.4) containing 1% glutaraldehyde and 4% paraformaldehyde overnight, then stored in 70% alcohol until ready for processing. Samples were stained in 1% osmium tetroxide for 60 min, then rinsed in increasing concentrations of ethanol up to 100%. Tissue was then rinsed in propylene oxide, then in increasing concentrations of epoxy resin in propylene oxide and finally embedded in 100% epoxy resin. Electron micrographs of cross-sections of the tissues were taken at 1,000x and 10,000x, then scanned into tagged image format files. Regions identified as containing contractile material were selected by the presence of hexagonal arrays of myofilaments, and their area calculated by construction of a polygon around the circumference of the region. The area of the polygon, A, can then be evaluated by defining the n vertices of a simple polygon in Cartesian coordinates, x and y, and forming the sum:

$$A = \frac{1}{2}\sum_{i=1}^{n}\left(x_i y_{i+1} - x_{i+1} y_i\right)$$

where the i+1 terms for i=n are taken as i=1, i.e. the polygon is closed. We evaluated the total area of all such regions and expressed it as a fraction of the area of the micrograph field.

In randomly selected sections containing myofibrillar tissue at x10000 magnification, the fractional myocyte cross-sectional area occupied by myofibrils was 0.508±0.035 (n=6, porcine) and 0.672±0.034 (n=8, human). In both tissues, an ordered myofilament lattice was present and there was no indication of damage to myofibrillar structure from ice crystallisation. The mean spacing between thick filaments was 29.7±0.7nm, compared to the unskinned spacing from porcine myocardium of 46.8±0.4nm, suggesting a shrinkage during fixation of 37%. In human tissue we found a lesser degree of uniformity in myofibril orientation; in different regions of the micrograph, myofilaments appeared either as cross-sections (i.e. points) or as a more filamentous structure, showing that the filament lattice had not been cut perpendicular to the axis of the myocytes. Fig. S6A shows an intercalated disk of human myocardium without evidence of disruption by ice crystallisation. At x1000 magnification in porcine myocardium, the fractional myocardial cross-sectional area occupied by myocytes was 0.762±0.035 (n=3, fig. S6B), so the fractional occupancy of the myocardium by myofibrils is 0.672x0.762 = 0.387. For human muscle at x1000, myocytes were less well defined. However, in two sections we could measure fractional occupancy of the myocardium by myofibrils directly for human tissue, obtaining 0.435 and 0.421. These data suggest that fractional occupancy of the myocardium by myofibrils is equal to ca. 0.4 in both porcine and human myocardium, in agreement with corresponding estimates from other species.

We also examined longitudinal sections from cryopreserved porcine muscle at x1000, x5000 and x10000. An example is shown in fig. S6C. These showed a regular sarcomere array without evidence of disruption by ice crystallisation as expected, since both human and

porcine tissue gave laser diffraction patterns. The short sarcomere length in these sections may also indicate considerable shrinkage during fixation, and so our estimate of fractional occupancy above must be based on the assumption that this shrinkage was uniform throughout the cross-section of the tissue.

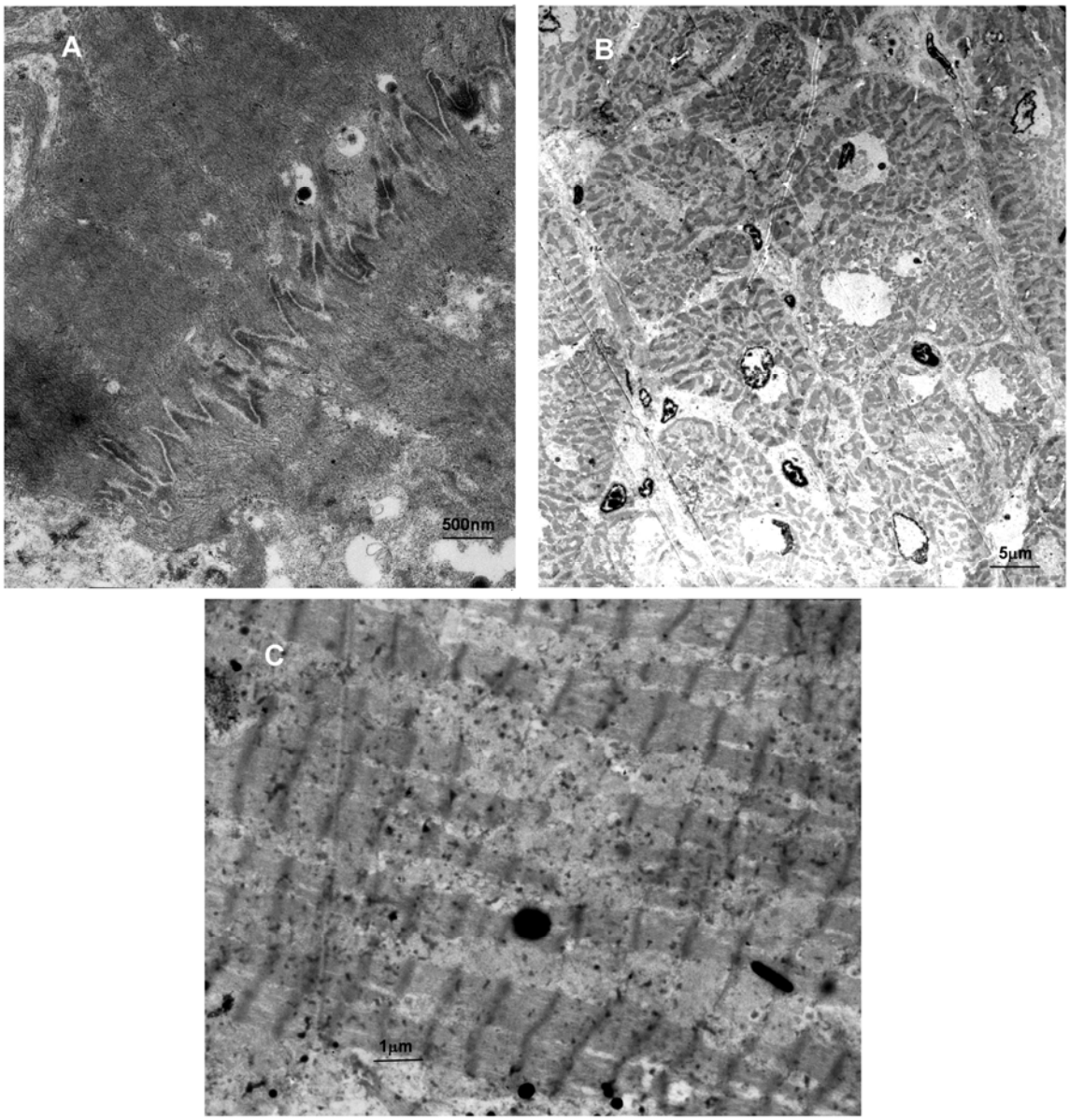

Figure S6: panel A; section through the intercalated disk (the diagonal 'zig-zag' structure running from top right to bottom left) of human myocardium showing fascia adherens (dark regions) and associated myofibrils. The disk appears to be unaffected by flash freezing. Sarcomere structures are only faintly evident because the section is not perfectly aligned along the longitudinal axis of the myocytes. Panel B; cross-section through flash frozen porcine myocardium showing myocytes containing myofibrils (dark regions) as discrete disks. The small, darker bodies present in small amounts throughout the section are mitochondria. Panel C; longitudinal section of porcine myocardium showing a well-ordered arrangement of sarcomeres and myofibrils. The very short

sarcomere length is probably a result of both shrinkage and contraction during fixation, since the preparation was not held between fixed ends.

S.5. X-ray diffraction measurements.

For X-ray measurements, the glass windows of the chambers were replaced by adjustable Kapton windows to permit passage of the X-ray beam (λ=0.15nm). The X-ray pattern was collected on a two dimensional MarCCD 165 X-ray detector (Marresearch GmbH, Hans-Böckler-Ring 17, 22851 Norderstedt, Germany) at a camera length of 3.25m at beamline A2, DESY, Hamburg. Exposure time was 20s. Data were analysed using user-designed software packages, and reflection intensities and spacing were calculated using a Marquardt-Levenberg fitting algorithm (6) described previously (7). Spacing measurements were calibrated using the M3 reflection from relaxed rabbit psoas skeletal muscle, taking the M3 spacing as 14.32nm. Chamber temperature for X-ray work was 6^{o}C.

We found that X-ray reflections from porcine or human myocardium are ca. 3-fold weaker than from a similar sized skeletal muscle preparation, but the most intense reflections are still easily resolved (fig. S7).

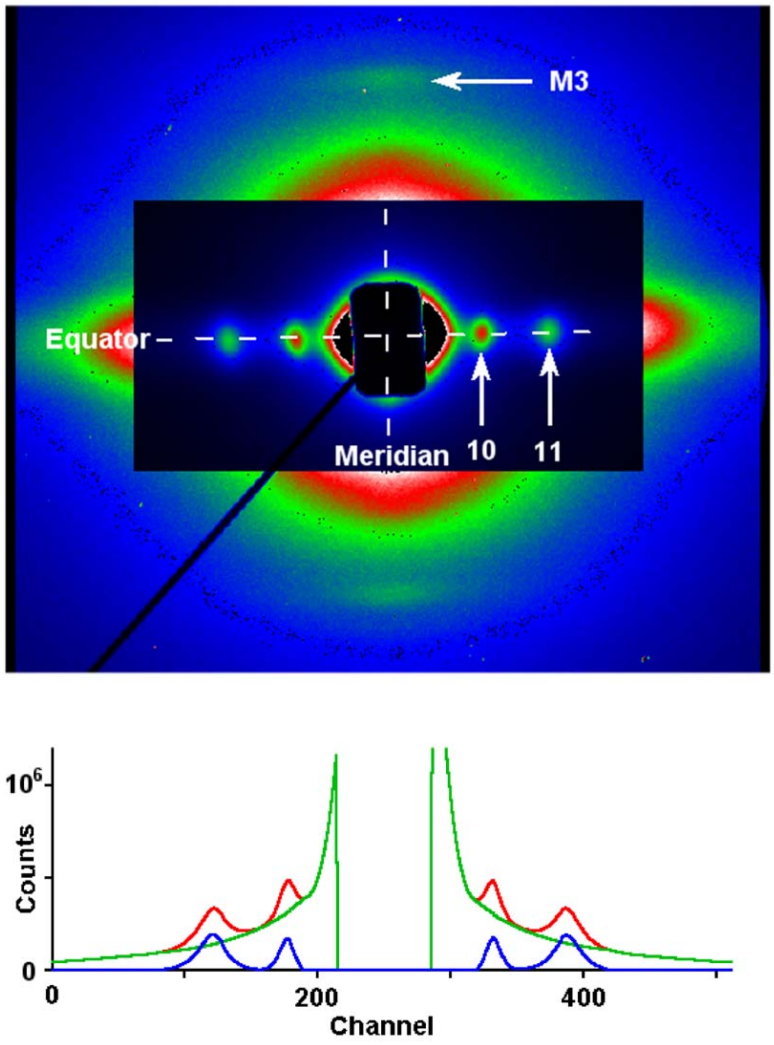

Figure S7: top panel: rigor X-ray diffraction pattern from glycerinated porcine myocardium. The pattern is displayed in false colours, dark blue being least, white most intense. The centre of the pattern is masked to reduce intensity by 90% to resolve the 10 and 11 equatorial reflections more clearly. The 10 intensity appears stronger than 11 because of the steep background intensity fall-off in the region of the backstop that was observed in all cardiac preparations. The meridional M3 reflection is also clearly visible. 20s exposure at 6°C, length 6mm, diameter 775μm. Bottom panel: equatorial intensity projection onto the equator between ±0.01nm^{-1} on the meridian (red trace). Background intensity (green trace) subtraction leaves the 10 and 11 reflections (blue trace), whose position and integrated intensity are then easily measurable. The centre to centre spacing of the myosin filaments (a) can then be computed as $2/(\sqrt{3}d_{10})$ or as $2/d_{11}$, where d_{10} and d_{11} are the distances of the 10 and 11 reflections from the centre of the pattern, measured in reciprocal space.

S.6. Mechanical Measurements.

Dynamic stiffness measurements were obtained from the force-extension plot generated from a single stretch and release (rise time 0.5ms). The force-extension plot was fitted to a linear regression of force upon length to obtain stiffness, and this was converted to Young's modulus using the maximum and minimum diameters of the preparation, assuming an ellipsoid cross-section. Static passive stiffness was obtained by stretching the relaxed preparations by a known fraction of their original length. The new sarcomere length was then calculated from the laser diffraction pattern. Expected and actual extension of sarcomere length agreed throughout the range of stretches applied. Because passive stiffness showed strong viscoelasticity, after each elongation of the preparation we waited 600s before recording tension or measuring dynamic stiffness, so as to allow passive tension to stabilise. Although some small tension decay was still present at the end of this period, it was deemed small enough to justify taking force as its final value.

The stiffness ratio in fig. 4 for human tissue is shifted to the right by about 0.1μm compared to glycerinated porcine muscle. This shift must be viewed with caution. Treating the bundle as a simple grating, sarcomere length was measured by directing the laser beam through the tissue at an angle, θ, such that the first order diffracted beam is emitted at 90° to the bundle axis. The distance, x, between zeroeth and first order beams at a plane of measurement parallel to the bundle is then $l \tan \theta$, where l is the path length from the bundle to the diffraction pattern plane. But if myocytes in the bundle were tilted by an angle (φ) relative to the bundle axis, then x becomes l (tan θ + tan (ψ-φ)), where sin ψ equals λ/s - sin (θ-φ) and s equals sarcomere length. We calculate that variation in φ by 20° can generate a sarcomere length error of up to 10%, ie. >0.2μm. Such a tilt could easily be achieved if a bundle were twisted or if the prevailing myocyte axes were not aligned with that of the bundle.

S.7. References.

1. Kentish, J. C. and G. J. M. Stienen. 1994. Differential effects of length on maximum force production and myofibrillar ATPase activity in rat skinned cardiac muscle. *J. Physiol. (Lond.).* 475:175-184.
2. Griffiths, P .J., K. Güth, H. J. Kuhn and J. C. Rüegg. 1980. ATPase activity in rapidly activated skinned muscle fibres. *Pflügers Arch.* 387:167-173.

3. Klotz, C., M. C. Aumont, J. J. Leger and B. Swynghedauw. 1975. Human cardiac myosin ATPase and light subunits. A comparative study. *Biochim. Biophys. Acta.* 386:461-469.
4. Kuhn, H. J., C. Bletz and J. C. Rüegg. 1990. Stretch-induced increase in the Ca^{2+} sensitivity of myofibrillar ATPase activity in skinned fibres from pig ventricles. *Pflügers Arch.* 415:741–746.
5. Narolska, N.A., R.B. van Loon, N.M. Boontje, R.Zaremba, S. Eiras Penas, et al. 2005. Myocardial contraction is 5-fold more economical in ventricular than in atrial human tissue. *Cardiovasc. Res.* 65: 221-229.
6. Press, W. H., B. P. Flannery, S. A. Teukolsky and W. T. Vetterling. 1990. Numerical recipes: the art of scientific computing. Cambridge University Press, Cambridge.
7. Griffiths, P. J., C. C. Ashley, M. A. Bagni, Y. Maéda and G. Cecchi, 1993. Cross-bridge attachment and stiffness during isotonic shortening of intact single muscle fibers. *Biophys. J*. 64:1150-1160.